Available online at website: https://journal.bcrec.id/index.php/bcrec

Bulletin of Chemical Reaction Engineering & Catalysis, 19 (4) 2024, 668-691

Research Article

Novel Study of Reaction Kinetics and Mass Transfer in Bioreactor Modelling: Prediction of Bioethanol Fermentation Performance by Saccharomyces cerevisiae on Continuous Fixed Bed Biofilm Plug Flow Reactor

Christian Aslan, Hary Devianto, Vita Wonoputri, Ardiyan Harimawan*

Department of Chemical Engineering, Faculty of Industrial Technology, Institut Teknologi Bandung, Bandung 40132, Indonesia

Received: 16th October 2024; Revised: 2nd December 2024; Accepted: 3rd December 2024
Available online: 5th December 2024; Published regularly: December 2024

Abstract

Bioethanol implementation as a renewable fuel has yielded economic, social, and environmental benefits, including reduced fossil fuel consumption, enhanced energy diversity and supply security, lower greenhouse gas emissions, and support for agricultural communities. These impacts underscore the importance of advancing innovation and optimizing processes to increase bioethanol production. Therefore, basic knowledge of chemical engineering in bioethanol fermentation is important to be learnt as a preliminary study, such as reaction kinetics and transport phenomena. This work studies the reaction kinetics and mass transfer in continuous fixed bed biofilm plug flow reactor modelling to predict anaerobic Saccharomyces cerevisiae fermentation performance, which is still not studied comprehensively. This modelling provides an overview of the influence of various independent variables, namely temperature, initial substrate concentration, cell concentration, superficial flow rate, reactor diameter, and solid particle diameter on various dependent variables, namely final product concentration, residence time, reactor length, reactor volume, product productivity, and pressure drop. The most sensitive parameters related to product productivity are temperature and cell concentration, so in its implementation, the temperature must be controlled at its optimum temperature, and the inoculum must be prepared with high cell concentration. For the next study, it is recommended to study the optimization of reactor design and operation (i.e. the pumping system, cooling system, and pH control of the reactor) and the implementation of the reactor on the plant scale.

Keywords: Bioethanol; bioreactor modelling; continuous fixed bed biofilm plug flow reactor; kinetic and mass transfer; Saccharomyces cerevisiae

How to Cite: Aslan, C., Devianto, H., Wonoputri, V., Harimawan, A. (2024). Novel Study of Reaction Kinetics and Mass Transfer in Bioreactor Modelling: Prediction of Bioethanol Fermentation Performance by Saccharomyces cerevisiae on Continuous Fixed Bed Biofilm Plug Flow Reactor. *Bulletin of Chemical Reaction Engineering & Catalysis*, 19 (4), 668-691 (doi: 10.9767/bcrec.20230)

Permalink/DOI: https://doi.org/10.9767/bcrec.20230

Supporting Information (SI): https://journal.bcrec.id/index.php/bcrec/article/downloadSuppFile/20230/5360

1. Introduction

Bioethanol or ethyl alcohol (C_2H_5OH) is a compound which can be obtained from the fermentation of simple sugars by yeast [1]. Bioethanol as renewable biofuel (fuel grade) is produced in the concentration of 99%-v [2] and can be utilized for the Otto cycle engine (gasoline engine) due to its similar characteristics to gasoline [3]. Bioethanol has several advantages, namely more environmentally friendly and higher-octane number [3,4].

Bioethanol is widely used in low-concentration gasoline blends (below E27) for regular cars and in high-concentration blends (E85) or pure form (E100) for flexible fuel vehicles, particularly in countries like the United States of America, Brazil, and European Union members. United States of America is the largest bioethanol producer (16,100 million gallons; 56%), primarily

* Corresponding Author.
Email: ardiyan@itb.ac.id (A. Harimawan)

using an E10 blend, while Brazil ranks as the second largest producer (7,950 million gallons; 28%), favoring the E27 blend. The European Union is the third largest producer (1,430 million gallons; 5%), with the members majorly using an E10 blend. The bioethanol developments in these countries have successfully provided economic, social, and environmental impacts, such as reducing fossil fuel consumption, increasing energy diversity, enhancing energy supply security, reducing greenhouse gas emissions, and supporting farmers. Hence, bioethanol presents a promising opportunity as a renewable fuel [5–9].

Studying innovations and optimizing production processes are essential steps to maximize bioethanol production. A thorough understanding of the thermodynamic and kinetic approach of chemical engineering related to bioethanol production is essential as a starting point, on a microscopic scale (cell) as well as macroscopic scale (bioreactor). On a microscopic scale, microorganisms perform a metabolism process, which can be simplified by unstructured and unsegregated model (black box model) [10]. This model is commonly used in the bioprocess industry because, despite its simplicity, it is already represented to calculate and predict biomass growth and product formation in a macroscopic scale system (bioreactor) [11]. In this model, the thermodynamics approach can be used to determine microbial stoichiometric reactions, which helps in identifying the C/N ratio, yield, fermentation efficiency, and heat production [12]. Meanwhile, the kinetic approach is used to identify the reaction time, which leads to bioreactor design (dimension) and productivity [13].

Currently, bioethanol is commercially produced by stirred tank bioreactor without cell immobilization, which can be performed batch or continuously with *Saccharomyces cerevisiae* as a biocatalyst [14–16]. Various efforts can be made to increase the productivity of ethanol, such as by changing the reactor configuration to a continuous fixed bed biofilm plug flow reactor. The biofilm reactor system (passive immobilization) has the advantages of increasing the reaction rate, increasing product productivity, and increasing cell concentration, as well as minimizing the need for cell recirculation [17]. Apart from that, the continuous plug flow reactor system also has advantages compared to the batch and continuous stirred tank reactor systems in terms of minimizing the number of shutdowns for cleaning the reactor between cycles, as well as shortening residence time and increasing productivity [18,19]. This shows that the continuous fixed bed biofilm plug flow reactor configuration has better advantages and has the potential to be developed.

Many studies regarding the kinetic approach on black box models have been conducted in various bioreactor applications, such as bioethanol and lactic acid [20–23]. However, the modelling of anaerobically bioethanol fermentation on continuous fixed bed biofilm plug flow reactor is still limited. Hence, this work uniquely addresses this gap by introducing a novel integration of reaction kinetics and mass transfer in black box bioreactor modelling to predict the performance of bioethanol fermentation by *S. cerevisiae* on a continuous fixed bed biofilm plug flow reactor. This study utilizes a mathematical model addressed through a numerical partial differential equation solver, offering insights that deepen understanding of bioethanol systems and potentially extend to a wide range of bioprocess applications.

2. Materials and Methods

2.1. Microbial Growth Kinetics in Biofilm

One of the microbial growth kinetics (including in biofilms) that is frequently used is the Monod equation, which is shown in Equation (1). The Monod equation is a semi-empirical equation that assumes that one type of enzyme with Michaelis-Menten kinetics is responsible for consuming substrate (*S*) because it has the slowest reaction rate and thus acts as a determinant of growth rate. In addition, this equation does not consider the rate of endogenous metabolism (metabolism for maintenance of cell structure) and the rate of microbial death [24].

$$\mu_g = \frac{\mu_{max} C_S}{K_S + C_S} \quad (1)$$

where, μ_g is specific microbial growth rate [h^{-1}], μ_{max} is maximum microbial growth rate [h^{-1}], K_S is half-velocity constant of microbes [g/L], and C_S is substrate concentration [g/L].

The Monod equation is then used to determine the growth rate of microorganisms, substrate consumption rate, and product formation rate. Assuming the microbial reaction follows Equation (2), then the growth rate of microorganisms is calculated by Equation (3). Furthermore, the rate of substrate consumption can be calculated from the growth rate of microorganisms and the yield of the number of microorganisms per amount of substrate, as shown in Equation (4). Meanwhile, the rate of product formation can also be calculated from the growth rate of microorganisms and the type of product formation, namely growth-associated product ($\alpha = Y_{P/X}$ = constant; $\beta = 0$), nongrowth-associated product ($\alpha = 0$; β = constant), and mixed-growth-associated product (α = constant; β = constant), as in Equation (5). The initial conditions for Equation (3) to Equation (5) are shown in Equation (6) to Equation (8) [24].

$$S \rightarrow X + P \quad (2)$$

$$r_X = \frac{dC_X}{dt} = \mu_g C_X = \frac{\mu_{max} C_S}{K_S + C_S} C_X \quad (3)$$

$$-r_S = \frac{dC_S}{dt} = \frac{1}{Y_{X/S}} \frac{dC_X}{dt} = \frac{1}{Y_{X/S}} \frac{\mu_{max} C_S}{K_S + C_S} C_X \quad (4)$$

$$r_P = \frac{dC_P}{dt} = \alpha \frac{dC_X}{dt} + \beta C_X = \alpha \mu_g C_X + \beta C_X = (\alpha \mu_g + \beta) C_X = q_P C_X \quad (5)$$

Initial conditions:

$$C_X = C_{X0} \text{ when } t = 0 \quad (6)$$

$$C_S = C_{S0} \text{ when } t = 0 \quad (7)$$

$$C_P = C_{P0} \text{ when } t = 0 \quad (8)$$

where: S is substrate, X is cell (biomass), P is product, r_X is cell production rate [g/(L.h)], r_S is substrate consumption rate [g/(L.h)],r_P is product production rate [g/(L.h)], t is time [s or min or h], $Y_{X/S}$ is biomass yield on substrate [g/g], $Y_{P/X}$ is product yield on biomass [g/g], α is growth-associated product constant [-], β is nongrowth-associated product specific production rate [h^{-1}], q_P is specific product production rate [h^{-1}], C_X is biomass concentration [g/L], C_P is product concentration [g/L], C_{X0} is initial biomass concentration [g/L], C_{S0} is initial substrate concentration [g/L], and C_{P0} is initial product concentration [g/L].

Note that these equations are commonly used for unsteady conditions that occur in a batch reactor, whereas biofilm reactors are mostly operated in steady state and continuous reactors. Therefore, these equations are used as a reference for compiling equations for continuous fixed bed biofilm plug flow reactor, by also considering aspects of transport phenomena.

2.2 Kinetics and Transport Phenomena in Continuous Fixed Bed Biofilm Plug Flow Reactor

Mass transfer in a continuous fixed bed plug flow biofilm reactor can be observed from two approaches, namely external mass transfer (substrate concentration profile in the reactor) and internal mass transfer (substrate concentration profile in the biofilm) on the substrate under steady conditions. In a continuous reactor, steady conditions are the desired conditions to obtain a stable rate and product concentration, and this condition can be achieved after some time after the reaction process is started (start-up).

2.2.1. External mass transfer

The substrate concentration profile and substrate mole mass balance of the continuous fixed bed biofilm plug flow reactor is shown in Figure 1. With the shell mass balance concept, the steady mass balance of the substrate component (S) in continuous fixed bed biofilm plug flow reactor is shown in Equation (9), which can be changed to Equation (10) [13].

$$F_{S,z} - F_{S,z+\Delta z} + r_S a_p A_R \Delta z = 0 \quad (9)$$

$$-\frac{1}{A_R}\left(\frac{\partial F_S}{\partial z}\right) + r_S a_p = 0 \quad (10)$$

where: z is directional dimension, F_S is substrate molecular flow rate [mole/s], $F_{S,z}$ is substrate molecular flow rate entering the shell at z position [mole/s], $F_{S,z+\Delta z}$ is substrate molecular flow rate exiting the shell at z+Δz position [mole/s], a_p is ratio of bed surface area to reactor volume [m^2/m^3], A_R is reactor cross-sectional area [m^2], and Δz is shell length [m].

In the plug flow reactor, the molecular diffusion of components in the axial direction can be assumed to be ignored, because their value is very small compared to the convection mass transfer (by the flow rate). Therefore, Equation (11), which reflects the substrate flux (affected by convection and diffusion), can be simplified to Equation (12) (affected by convection only) [25].

$$F_S = A_R W_S = A_R (J_S + u_z C_S) \quad (11)$$

$$F_S = A_R u_z C_S \quad (12)$$

where, W_S is total flux [g/(m^2.s)], J_S is molecular flux of substrate [g/(m^2.s)], u_z is fluid superficial flow rate throughout reactor [m/s].

In a steady system, the reaction rate of substrate consumption on the biofilm surface is equal to the substrate mass flux from the bulk phase to the biofilm surface. Therefore, the rs value can be calculated using Equation (13).

$$F_S = A_R u_z C_S \quad (13)$$

where, $C_{SB,i}$ is substrate concentration at the biofilm surface [g/L] and k_S is substrate mass transfer coefficient [m/s]. Next, Equation (14) is obtained by substituting Equation (12) and Equation (13) into Equation (10). Equation (14) can be solved with the boundary conditions shown in Equation (15).

$$u_z \frac{\partial C_S}{\partial z} + k_S a_p (C_S - C_{SB,i}) = 0 \quad (14)$$

Boundary condition: $C_S = C_{S0}$ at $z = 0$ (15)

To ease the modeling, the variable z is changed to residence time (τ). Equation 16 shows the equation to calculate the residence time as a z variable, which can be reduced to Equation (17).

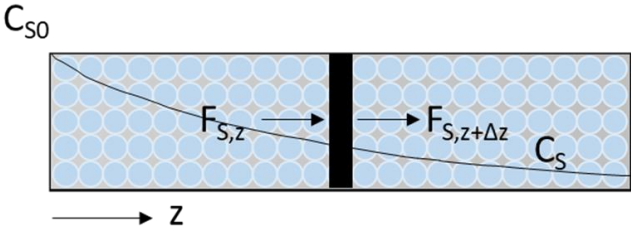

Figure 1. Substrate concentration profile and shell mass balance in continuous fixed bed biofilm plug flow reactor.

Equation (17) is then substituted into Equation (14) to obtain Equation (18). Then, the boundary condition in Equation (15) is changed to the initial conditions in Equation (19) [13].

$$\tau = \varepsilon \frac{V_R}{\dot{V}} = \varepsilon \frac{A_R L}{A_R u_z} = \varepsilon \frac{L}{u_z} = \varepsilon \frac{z}{u_z} \quad (16)$$

$$\partial z = \frac{u_z}{\varepsilon} \partial \tau \quad (17)$$

$$\varepsilon \frac{\partial C_S}{\partial \tau} + k_S a_p \left(C_S - C_{SB,i}\right) = 0 \quad (18)$$

$$\text{Boundary condition: } C_S = C_{S0} \text{ at } \tau = 0 \quad (19)$$

where, τ is reactor residence time [s or min or h], ε is void fraction [-], V_R reactor volume [m^3], $\dot{V}$ is volumetric fluid flow rate [m^3/s], and L is reactor length [m].

2.2.2 Internal mass transfer

The substrate concentration profile on the surface and inside the biofilm is shown in Figure 2. Microscopically, there are two areas examined, namely the diffusion layer and the biofilm. The equation to calculate the substrate concentration on the biofilm surface is shown in Equation (20), which occurs on the biofilm surface under steady conditions. To simplify the model, this study assumes that the biofilm thickness is constant (the growth and detachment rate of the biofilm is equal). Under steady conditions, the substrate diffusion rate is equal to the substrate consumption rate [24]. Equation (20) can be converted into Equation (21) and calculated by solving the quadratic equation shown in Equation (22) (a value), Equation (23) (b value), Equation (24) (c value), and Equation (25) (positive root value).

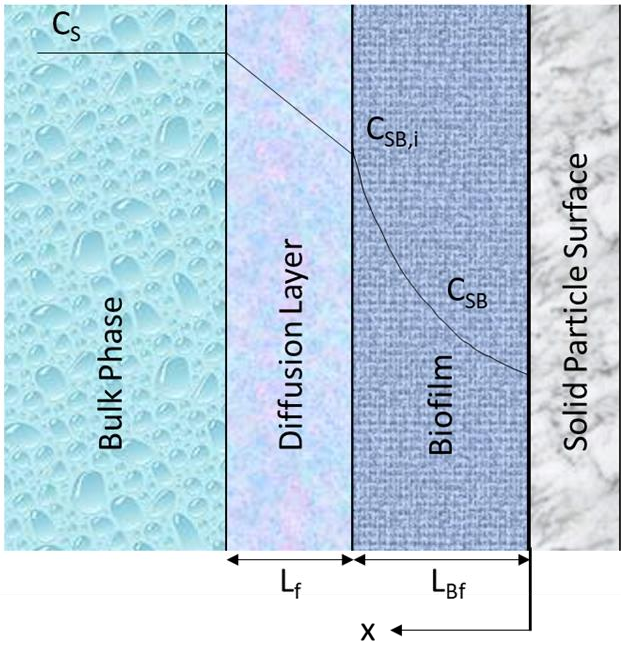

Figure 2. Substrate concentration profile inside the diffusion layer and the biofilm.

$$k_S a_p \left(C_S - C_{SB,i}\right) = \frac{q_P C_X}{Y_{P/S}} \frac{\mu_{max} C_{SB,i}}{K_{SB} + C_{SB,i}} C_X f(P) \quad (20)$$

$$(k_S a_p) C_{SB,i}^2 + \left(k_S a_p K_{SB} + \frac{Y_{P/X}}{Y_{P/S}} \mu_{max} C_X - k_S a_p C_S\right) C_{SB,i} + \left(-k_S a_p C_S K_{SB}\right) = 0 \quad (21)$$

$$a = k_S a_p \quad (22)$$

$$b = k_S a_p K_{SB} + \frac{Y_{P/X}}{Y_{P/S}} \mu_{max} C_X f(P) - k_S a_p C_S \quad (23)$$

$$c = -k_S a_p C_S K_{SB} \quad (24)$$

$$C_{SB,i} = \frac{-b + \sqrt{b^2 - 4ac}}{2a} \quad (25)$$

where, $Y_{P/S}$ is product yield on substrate [g/g], $f(P)$ is product inhibition factor [-], K_{SB} is half velocity constant of biofilm [g/L], and a, b, c are calculated value used to calculate substrate concentration at the biofilm surface [s^{-1}].

Mass transfer in the biofilm is identified using the continuity equation table in Bird [25], which is shown in Equation (26). This study uses Cartesian coordinates because the thickness of the biofilm is much smaller than the diameter of the bed. The substrate consumption rate value is approximated from the product formation rate value, which is shown in Equation (27). Ethanol is considered a growth-associated product [26] so Equation (27) can be changed to Equation (28). Under steady conditions and by substitution in Equation (28), Equation (26) is changed to Equation (29), with 2 boundary conditions shown in Equation (30) and Equation (31).

$$\frac{\partial C_{SB}}{\partial t} + u_x \frac{\partial C_{SB}}{\partial x} + u_y \frac{\partial C_{SB}}{\partial y} + u_z \frac{\partial C_{SB}}{\partial z} = D_e \left(\frac{\partial^2 C_{SB}}{\partial x^2} + \frac{\partial^2 C_{SB}}{\partial y^2} + \frac{\partial^2 C_{SB}}{\partial z^2}\right) + r_{SB} \quad (26)$$

$$-r_{SB} = \frac{q_P C_X}{Y_{P/S}} f(P) \quad (27)$$

$$-r_{SB} = \frac{Y_{P/X}}{Y_{P/S}} \frac{\mu_{max} C_{SB}}{K_{SB} + C_{SB}} C_X f(P) \quad (28)$$

$$D_e \frac{\partial^2 C_{SB}}{\partial x^2} = \frac{Y_{P/X}}{Y_{P/S}} \frac{\mu_{max} C_{SB}}{K_{SB} + C_{SB}} C_X f(P) \quad (29)$$

$$\text{First boundary condition: } C_{SB} = C_{SB,i} \text{ at } x = 0 \quad (30)$$

$$\text{Second boundary condition: } \frac{\partial C_{SB}}{\partial x} = 0 \text{ at } x = L_{Bf} \quad (31)$$

where, u_x, u_y, u_z are fluid superficial flow rate to a certain direction [m/s], x, y, z are directional dimensions, D_e is substrate diffusivity in the biofilm [m^2/s], r_{SB} is substrate consumption in biofilm [g/(L.h)], and L_{Bf} is biofilm thickness [m].

Several variables above are calculated using Equation (32) to Equation (42). Equation (32) is an equation to calculate the cross-sectional area (base) of the reactor, which is calculated using the area of the circle. Equation (33) is the void fraction value as a function of the ratio between the reactor diameter and the particle diameter for the spherical particle [27]. Equation (34) is the ratio of bed surface area to reactor volume [25]. Equation (35) is an equation to calculate the diffusivity of the substrate in the bulk phase, known as the Wilke-Chang correlation [28]. Equation (36) is an equation to calculate substrate

diffusivity in biofilm [29]. Equation (37) is an equation to calculate the Reynolds number [25]. Equation (38) is an equation to calculate the Schmidt number [25]. Equation (39) is an equation to calculate the Colburn factor as a function of the Reynolds number and void fraction [13]. Equation (40) is an equation to calculate the Sherwood number as a function of the Colburn factor, Reynolds number, and Schmidt number [13]. Equation (41) is an equation to calculate the mass transfer coefficient in the reactor [28]. Equation (42) is an equation to calculate biofilm thickness as a function of cell concentration, cell density, and the ratio of bed surface area to reactor volume.

$$A_R = \frac{\pi d_R^2}{4} \quad (32)$$

$$\varepsilon = 0.390 + \frac{1.740}{\left(\frac{d_R}{d_p}+1.140\right)^2} \quad (33)$$

$$a_p = 6\frac{(1-\varepsilon)}{d_p} \quad (34)$$

$$D_{aq} = 1.173 \times 10^{-16}\left(\phi_{solvent} M_{r,solvent}\right)^{1/2} \frac{T}{\mu_{solvent} V_{solute}^{0.6}} \quad (35)$$

$$D_e = c_{dif} \times D_{aq} \quad (36)$$

$$Re = \frac{\rho_f u_z d_p}{\mu_f} \quad (37)$$

$$Sc = \frac{\mu_f}{\rho_f D_{aq}} \quad (38)$$

$$J_D = \frac{1}{\varepsilon}\left(\frac{0.765}{Re^{0.82}} + \frac{0.365}{Re^{0.386}}\right) \quad (39)$$

$$Sh = J_D Re Sc^{1/3} \quad (40)$$

$$k_S = \frac{Sh D_{aq}}{d_p} \quad (41)$$

$$L_{Bf} = \frac{C_X}{a_p \rho_X} \quad (42)$$

where, d_R is reactor diameter [m], d_p is solid particle diameter [m], $D_{aq}$is substrate diffusivity in the bulk phase [m^2/s], $\phi_{solvent}$ is association parameter of solvent (water) [-], $M_{r,solvent}$ is molecular mass of solvent (water) [g/mole], T is temperature [K], $\mu_{solvent}$ is solvent (water) dynamic viscosity at a certain temperature [Pa.s], V_{solute} is solute (substrate) molecular volume [m^3/kmole], c_{dif} is ratio of diffusivity of solute (substrate) in biofilm and diffusivity of solute (substrate) in bulk phase [-], D_e is substrate diffusivity in the biofilm [m^2/s], Re is Reynold number of the reactor [-], ρ_f is fluid density [kg/m^3], μ_f is fluid dynamic viscosity (water) at a certain temperature [Pa.s], Sc is Schmidt number of the reactor [-], J_D is Colburn factor of mass transfer [-], Sh is Sherwood number of the reactor [-], and ρ_X is cell density [kg/m^3].

2.3 Model and Basis of the Simulation Study

This study was carried out by a numerical partial differential equations simulator to identify the performance of the reactor. In this study, ethanol produced by *S. cerevisiae* is considered as a growth-associated product [26]. Then, the rate of cell production does not change the thickness of the biofilm (the number of cells formed in the biofilm is the same as the number of cells detached from the biofilm). Moreover, the physical properties of the fluid (density and viscosity) are assumed to be the physical properties of water at the fermentation temperature. For the kinetics, the effect of pH and substrate inhibition were ignored, while product inhibition was considered because ethanol is a toxic product and can inhibit growth. The maximum specific growth rate of microorganisms and the product inhibition factor are calculated using Equation (43) [12,30] and Equation (44) [11], respectively.

$$\mu_{max} = \frac{A\exp\left(-\frac{E_g}{RT}\right)}{1+B\exp\left(-\frac{\Delta G_d}{RT}\right)} \quad (43)$$

$$f(P) = 1 - \frac{C_P}{C_{P,max}} \quad (44)$$

where, A and B are pre-exponential constant [-], E_g is activation energy of microorganism growth [J/mole], ΔG_d is Gibbs free energy of protein denaturation [J/mole], R is gas constant [J/(mole.K)], and $C_{P,max}$ is maximum ethanol concentration [g/L].

The parameters used for modeling are shown in Table 1 and Table 2. These parameters consist of reactor and bed design, operation, fluid hydrodynamics and transport phenomena, reaction kinetics, and cell physical properties. The default conditions are temperature of 31 ^{o}C, substrate concentration 100 g/L, cell concentration of 10 g/L, superficial flow rate of 3.2 cm/s (equals to volumetric flow of 1 L/s), reactor diameter of 20 cm, and solid particle diameter of 20 mm.

This study was carried out by numerical partial differential equations solver (FlexPDE6) to understand the performance of the reactor in the form of the substrate concentration as a function of residence time, which is used to determine the final substrate concentration, reactor length, reactor volume, final product concentration, product productivity, and pressure drop. Equation (45) until Equation (50) are used to determine the final substrate concentration, reactor length, reactor volume, final product concentration, product productivity, and pressure drop, respectively. Note that the pressure drop equation (Equation (50)) can be used in laminar, transition or turbulent regimes [28].

$$C_{Sf} = (1 - X_S)C_{S0} \quad (45)$$

$$L = \frac{\tau u_z}{\varepsilon} \quad (46)$$

$$V_R = A_R L = \frac{\pi d_R^2}{4} L \quad (47)$$

$$C_{Pf} = Y_{P/S}(C_{S0} - C_{Sf}) \quad (48)$$

Table 1. Parameters used for continuous fixed bed biofilm reactor modeling

No.	Parameter	Value	Explanation
Bed and reactor design			
1	Reactor length (L) [m]	Calculated	As Equation (16) (or Equation (46))
2	Inner diameter of reactor (d_R) [cm]	Varied	10; 15; 20; 25; 30
3	Solid particle shape	Spherical	Assume solid spherical
4	Solid particle diameter (d_p) [mm]	Varied	10; 15; 20; 25; 30
5	Bed porosity (ε) [-]	Calculated	As Equation (33)
Operation			
6	Fermentation temperature (T) [^oC]	Varied	5-40 ^oC
7	Fermentation pressure (p) [atm]	1	Atmospheric pressure
8	Fermentation mode	Anaerobic	Enhance ethanol production
9	Initial substrate concentration (C_{S0}) [g/L]	Varied	50; 75; 100; 125; 150
10	Cell concentration [C_X] [g/L]	Varied	3.75; 5.63; 7.50; 9.38; 11.25
11	Feed volumetric flow ($\dot{V}$) [L/s]	Varied	0.50; 0.75; 1.00; 1.25; 1.50
12	Superficial flow rate (u_z) [cm/s]	Calculated from ($\dot{V}$)	1.6; 2.4; 3.2; 4.0; 4.8
13	Conversion (X_S)	99%	Assume almost 100% conversion
14	Steady/unsteady state	Steady	No accumulation in the reactor
Fluid hydrodynamics and transport phenomena			
15	Water density (ρ_f) [kg/m^3]	Calculated	[28]
16	Water viscosity (μ_f) [Pa.s]	Calculated	[28]
17	Glucose diffusivity in bulk phase (D_{aq}) [m^2/s]	Calculated	As Equation (35)
18	Ratio of diffusivity of glucose in biofilm and diffusivity of glucose in bulk phase (c_{dif}) [-]	0.3	[29]
19	Glucose diffusivity in biofilm (D_e) [m^2/s]	Calculated	As Equation (36)
20	Mass transfer coefficient of glucose (k_S) [m/s]	Calculated	As Equation (41)
Reaction kinetics			
21	Half velocity constant of biofilm (K_{SB}) [mg/L]	150	[11]
22	Pre-exponential constant A (A) [-]	8.9877×10^{18}	[30]
23	Pre-exponential constant B (B) [-]	5.8935×10^{50}	[30]
24	Activation energy of microorganism growth (E_g) [J/mole]	111,900	[30]
25	Gibbs free energy of protein denaturation (ΔG_d) [J/mole]	296,900	[30]
26	Gas constant (R) [J/(mole.K)]	8.314	[30]
27	Maximum specific growth rate of microorganism (μ_{max}) [h^{-1}]	Table 2	[12,30]
28	Maximum ethanol concentration ($C_{P,max}$) [(g/L]	170	[11]
29	Product yield on substrate ($Y_{P/S}$) [g/g]	Table 2	[12]
30	Product yield on biomass ($Y_{P/X}$) [g/g]	Table 2	[12]
Cell physical properties			
31	Cell density [g/mL]	1.0952	[36]

Table 2. Maximum specific growth rate of microorganism, product yield on substrate, and product yield on biomass [12]

T (^oC)	μ_{max} (h^{-1})	$Y_{P/S}$ (g/g)	$Y_{P/X}$ (g/g)
5	0.008	0.447	4.559
10	0.020	0.443	4.242
15	0.045	0.440	4.020
20	0.100	0.437	3.863
22.5	0.146	0.436	3.806
25	0.207	0.435	3.764
27	0.264	0.435	3.745
29	0.315	0.435	3.748
31	0.339	0.436	3.787
33	0.320	0.438	3.892
35	0.262	0.441	4.117
37.5	0.176	0.449	4.726
40	0.108	0.461	6.086

$$P_{Pf} = \frac{C_{Pf}}{\tau} \quad (49)$$

$$\Delta p = \frac{150\mu_f u_z L}{d_p^2}\frac{(1-\varepsilon)^2}{\varepsilon^3} + \frac{1.75\rho_f u_z^2 L}{d_p}\frac{1-\varepsilon}{\varepsilon^3} \quad (50)$$

where, C_{Sf} is final substrate concentration [g/L], X_S is substrate conversion [%], C_{Pf} is final product concentration [g/L], and P_{Pf} is product productivity at a certain conversion [g/(L.h)], and Δp is pressure drop [Pa].

3. Results and Discussion

3.1. Comparison with Stirred Tank Reactor Without Cell Immobilization

The process commonly used in industry for bioethanol production is a stirred tank reactor without immobilization, which can be operated either as a batch or continuous process. A comparison between the stirred tank reactor without immobilization and the continuous fixed bed plug flow biofilm reactor is shown in Table 3, concerning the residence time, cell concentration, reactor volume, and productivity.

The residence time values from lowest to highest are continuous fixed bed plug flow biofilm reactor, batch stirred tank reactor without immobilization, and continuous stirred tank reactor without immobilization. This shows that the continuous fixed bed plug flow biofilm reactor has an advantage in residence time (higher reaction rate). Continuous fixed bed plug flow biofilm reactor has a higher reaction rate because the surface area of the packing inside the reactor increases the cell density. Lower residence time (higher reaction rate) in the continuous fixed bed biofilm reactor leads to higher productivity values.

Based on Table 3, the reactor volume values from lowest to highest are batch stirred tank reactor without immobilization, continuous stirred tank reactor without immobilization, and continuous fixed bed plug flow biofilm reactor. In stirred tank reactors without immobilization, the continuous system requires a larger volume compared to the batch system. This is because, in a continuous and steady-state system, the reaction rate occurs at very low substrate concentrations—specifically, at the reactor's output concentration, where 99% conversion is achieved. On the other hand, the continuous fixed bed plug flow biofilm reactor also necessitates a larger volume due to the bed filling within the reactor. However, the amount of biocatalyst required in the continuous fixed bed plug flow biofilm reactor is lower compared to other reactor types. This indicates that the fixed bed reactor performs more efficiently in terms of biocatalyst utilization.

Overall, the continuous fixed bed plug flow biofilm reactor has better productivity, smaller residence time, and minimum biocatalyst requirement compared to other configurations. This shows that the fixed bed pipe continuous-biofilm reactor has better potential for further development. However, the required reactor volume in continuous fixed bed plug flow biofilm reactor remains higher than in other configurations. Therefore, further research is needed to optimize operating conditions and identify the most sensitive parameters that significantly impact the design and performance of continuous fixed bed plug flow biofilm reactors.

3.2 Influence of Various Parameters on Reactor Design and Performance

Several input parameters were identified for their impact on reactor design and performance, including temperature, substrate concentration, cell concentration, superficial flow rate, reactor diameter, and solid particle diameter. The corresponding output parameters affecting reactor design and performance include product concentration, residence time, reactor length, reactor volume, product productivity, and pressure drop.

3.2.1 Influence of temperature on reactor design and performance

The influence of fermentation temperature on reactor design and performance is shown in Figure 3 (Table S1, Supporting Information (SI)). Based on Figure 3(a), Figure 3(b), Figure 3(c),

Table 3. Comparison of the design and performance of a stirred tank reactor without immobilization with a continuous fixed bed plug flow biofilm reactor

Configuration	Reaction or Residence Time (minute)	Reactor Volume (m^3)	Cell Concentration (g/L)	Productivity (g/(L.hour))
Batch stirred tank reactor without immobilization	185.6	11.1	Initial: 7.5 Final: 18.9 Mean: 13.2	13.9
Continuous stirred tank reactor without immobilization	272.8	16.4	Steady: 10.9	9.5
Continuous fixed bed plug flow biofilm reactor	126.7	18.8	Fixed bed: 7.50	20.6

Figure 3(d), and Figure 3(f) the lowest values for residence time, reactor length, reactor volume, and pressure drop are obtained when the fermentation temperature of 31 °C. Meanwhile, the values for residence time, reactor length, reactor volume, and pressure drop increase at higher or lower temperatures. The temperature of 31 °C is the optimum growth temperature for *S. cerevisiae* [30]. This shows that the reactor design is greatly influenced by the fermentation temperature. The temperature is sensitive to cell growth rate because cell activities correspond to the enzyme activities, and enzyme activities depend significantly on temperature. If the microbial growth rate is higher, the residence time and reactor size will be smaller.

However, as shown in Figure 3(b), the highest product concentration value is achieved when the fermentation temperature is 40 °C, which is not the optimum temperature for *S. cerevisiae*. At its optimum temperature, microorganisms tend to use the substrate for growth rather than product formation [30]. However, examining the productivity values (Figure 3(e)) reveals that the highest productivity is achieved at the optimum temperature of 31°C. This indicates that in the

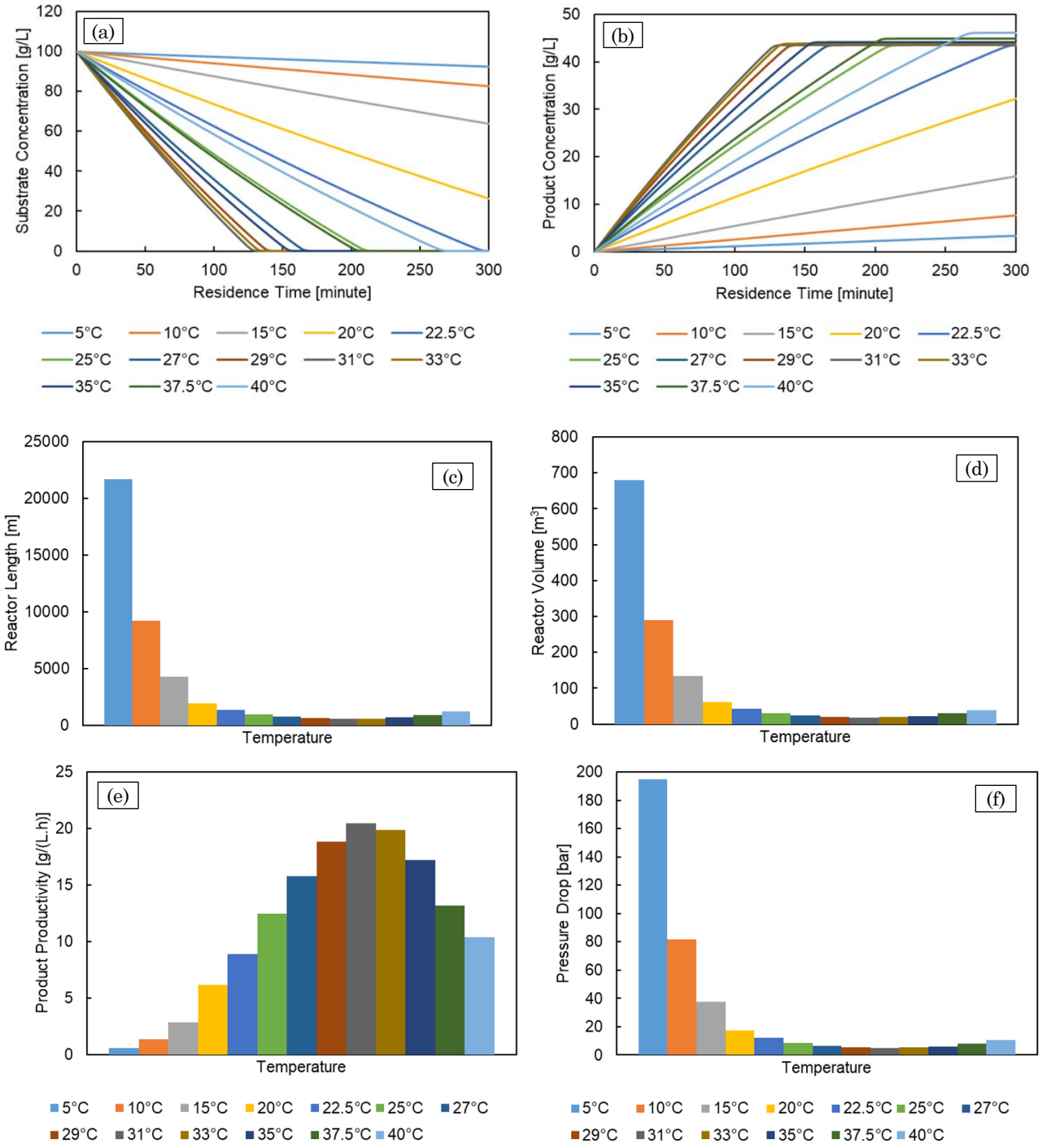

Figure 3. Influence of temperature on: (a) substrate concentration profile, (b) product concentration profile, (c) reactor length at 99% conversion, (d) reactor volume at 99% conversion, (e) product productivity at 99% conversion, and (f) pressure drop at 99% conversion

production process, the reaction rate, which is closely related to residence time and reactor size, is more crucial than the product yield.

3.2.2. Influence of initial substrate concentration on reactor design and performance

The influence of initial substrate concentration on reactor design and performance is shown in Figure 4 (Table S2, Supporting Information (SI)). The residence time (Figure 4(a)), final product concentration, (Figure 4(b)), reactor length (Figure 4(c)), reactor volume (Figure 4(d)), and pressure drop (Figure 4(f)) are directly proportional to the initial substrate concentration. When the initial substrate concentration is increased, the time required to convert the substrate into a product also increases, which leads to an increase in reactor length and reactor volume. Additionally, the increase in reactor length result in the increase of the pressure drop.

Productivity (Figure 4(e)) is inversely proportional to the initial substrate concentration. At high initial glucose concentrations, the rate of ethanol formation will also increase, which is in accordance with Monod kinetics. However, as time continues, the ethanol concentration increases, and due to the toxic properties of ethanol toward microbes, cell growth is inhibited, and ethanol formation is halted [11].

3.2.3 Influence of cell concentration on reactor design and performance

Figure 5 (Table S3, Supporting Information (SI)) illustrates the impact of cell concentration on reactor design and performance. As shown, residence time (Figure 5(a) and Figure 5(b)), reactor length (Figure 5(c)), reactor diameter (Figure 5(d)), and pressure drop (Figure 5(f)) are inversely proportional to cell concentration, while productivity (Figure 5(e)) is directly proportional. This occurs because a higher biocatalyst concentration increases the reaction rate of

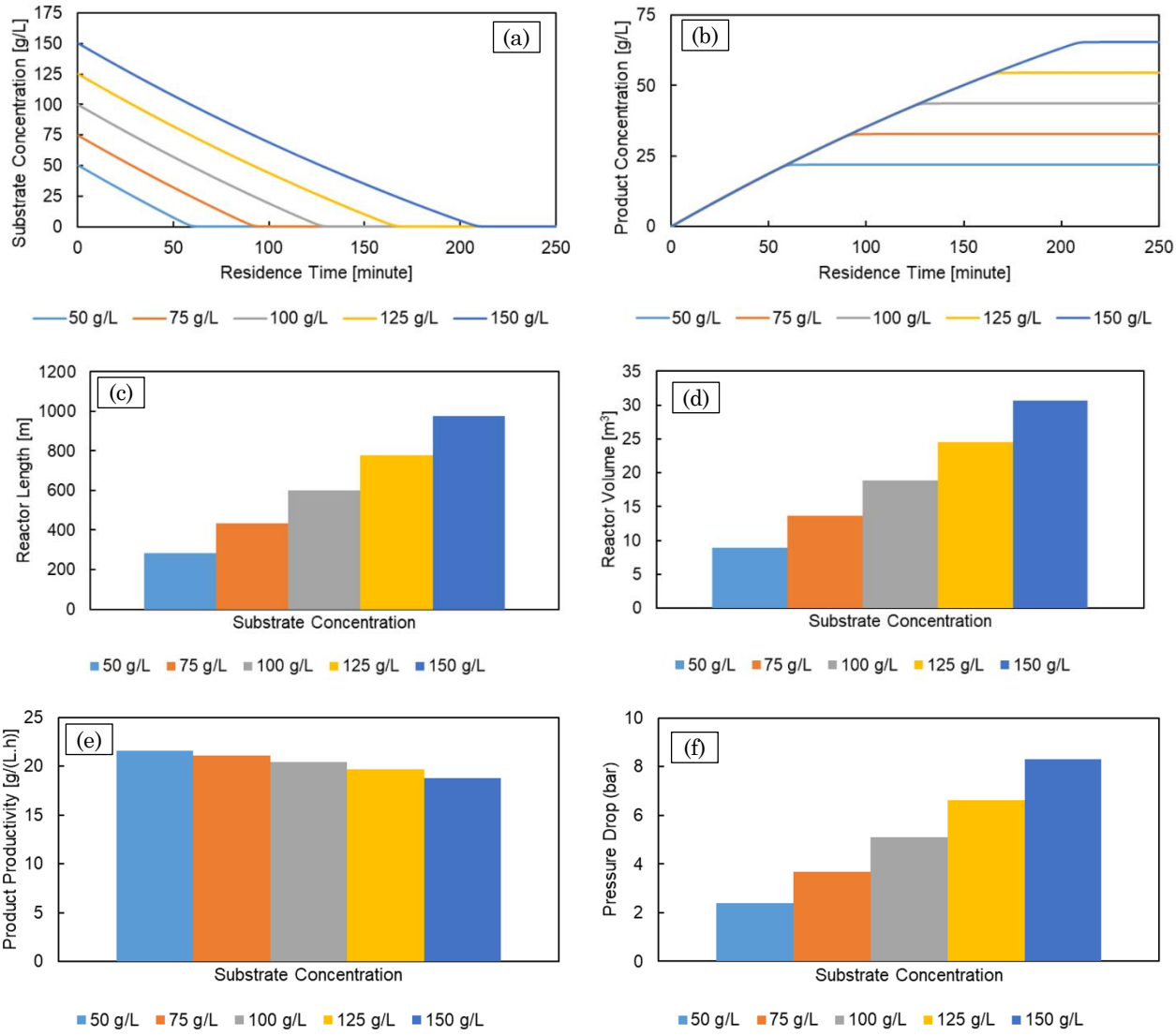

Figure 4. Influence of initial substrate concentration on (a) substrate concentration profile, (b) product concentration profile, (c) reactor length at 99% conversion, (d) reactor volume at 99% conversion, (e) product productivity at 99% conversion, and (f) pressure drop at 99% conversion.

product formation [24], resulting in reduced residence time, reactor length, reactor volume, and pressure drop, while increased productivity.

3.2.4 Influence of superficial flow rate on reactor design and performance

The influence of superficial flow rate on reactor design and performance is shown in Figure 6 (Table S4, Supporting Information (SI)). The differences in residence time (Figure 6(a) and Figure 6(b)) and productivity (Figure 6(e)) due to variations in superficial flow rate were minimal, indicating that the mass transfer rate is faster than the substrate conversion rate.

Although the superficial flow rate does not affect the residence time and productivity, the superficial flow rate still affects the reactor dimensions, namely reactor length (Figure 6(c)) and reactor volume (Figure 6(d)). As the superficial flow rate increases, the contact time of the substrate with the biocatalyst will be reduced, necessitating a longer reactor and larger reactor volume to maintain effective substrate conversion, resulting in higher pressure drop (Figure 6(f)).

3.2.5 Influence of reactor diameter on reactor design and performance

The influence of reactor diameter on reactor design and performance is shown in Figure 7 (Table S5, Supporting Information (SI)) at a constant superficial flow rate. Reactor diameter is inversely proportional to the void fraction (Table S5). This occurs because the void fraction is influenced by the ratio of reactor diameter to solid particle diameter (Equation 33). If the ratio is lower (lower reactor diameter), then the void fraction will be higher. This difference in void fraction values will also affect the length, volume, and performance of the reactor.

Based on Figure 7, the residence time (Figure 7(a) and Figure 7(b)) value is inversely

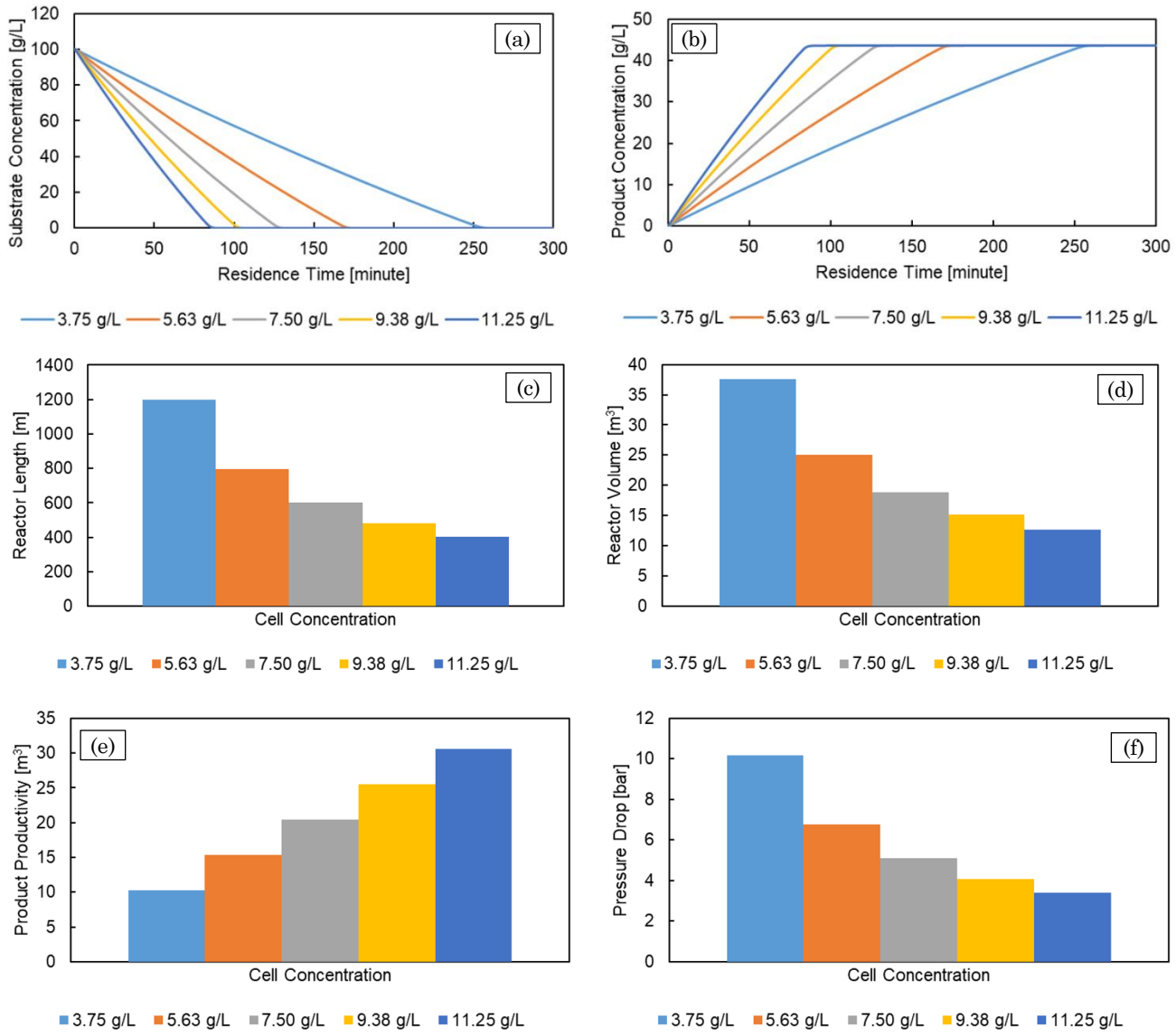

Figure 5. Influence of cell concentration on (a) substrate concentration profile, (b) product concentration profile, (c) reactor length at 99% conversion, (d) reactor volume at 99% conversion, (e) product productivity at 99% conversion, (f) and pressure drop at 99% conversion.

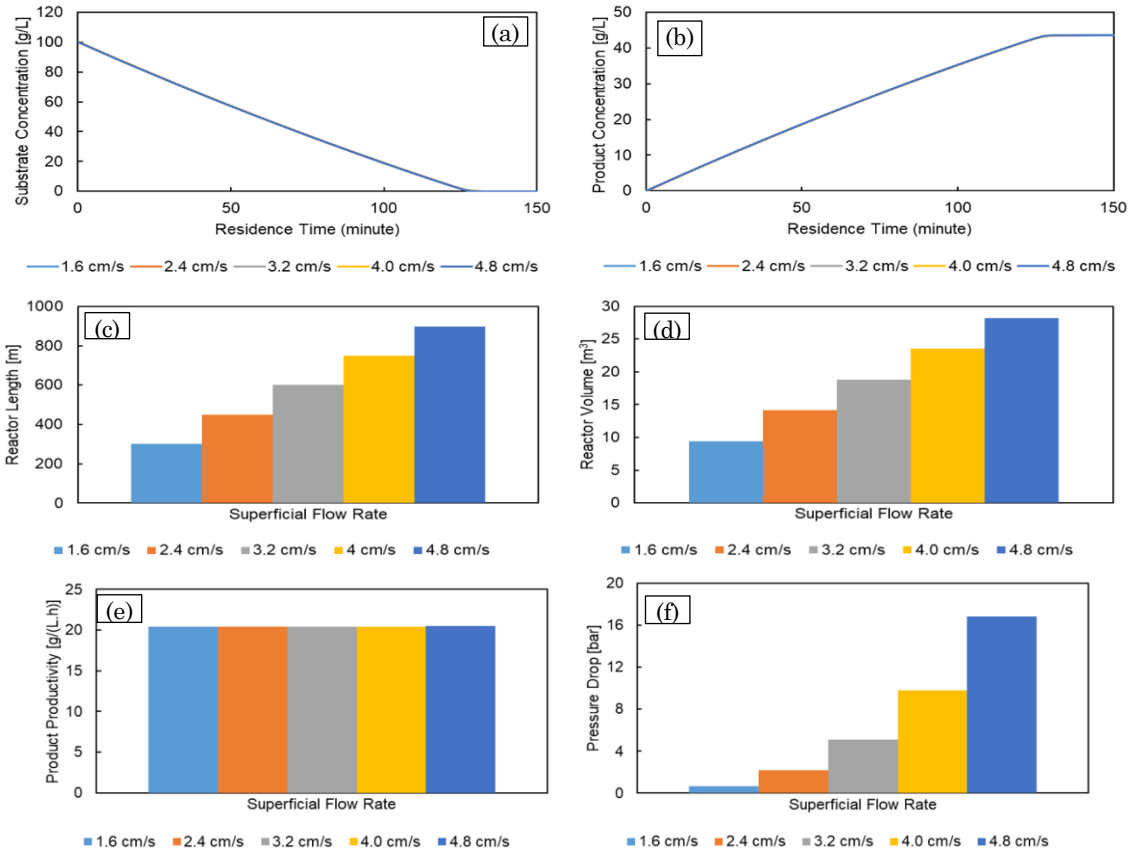

Figure 6. Influence of superficial flow rate on (a) substrate concentration profile, (b) product concentration profile, (c) reactor length at 99% conversion, (d) reactor volume at 99% conversion, (e) product productivity at 99% conversion, and (f) pressure drop at 99% conversion.

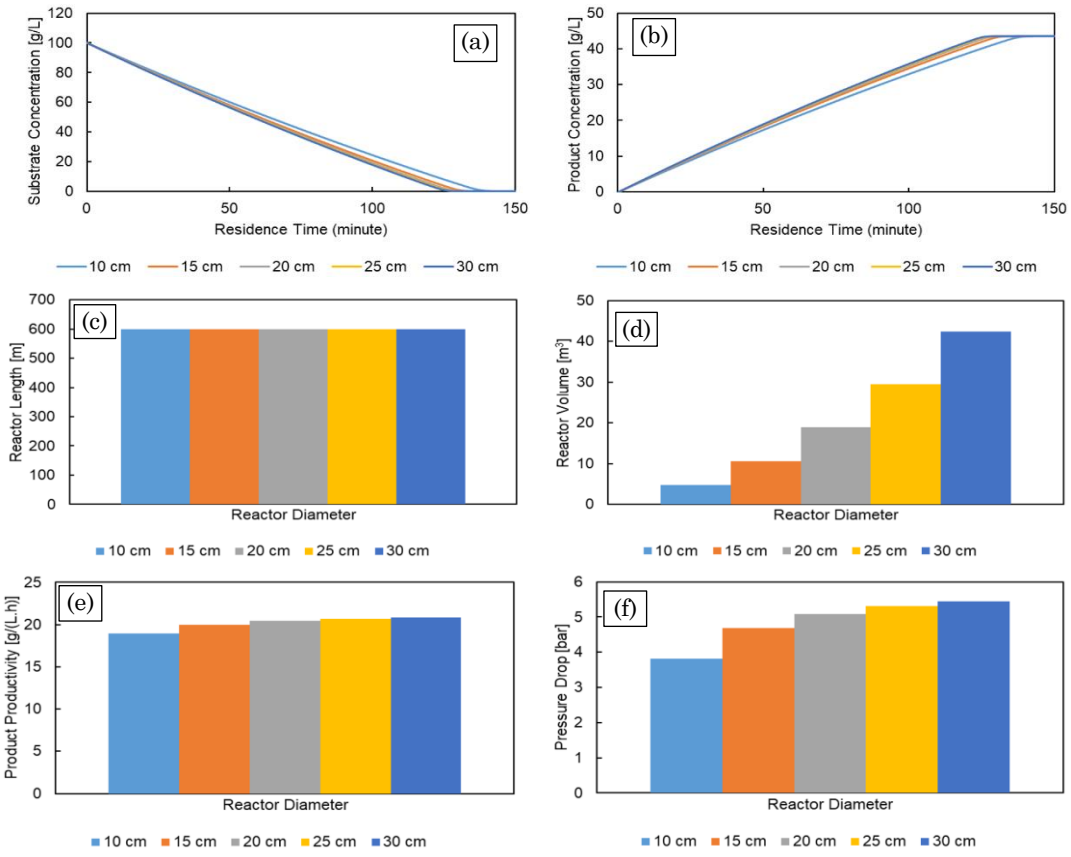

Figure 7. Influence of reactor diameter on (a) substrate concentration profile, (b) product concentration profile, (c) reactor length at 99% conversion, (d) reactor volume at 99% conversion, (e) product productivity at 99% conversion, and (f) pressure drop at 99% conversion.

proportional to the reactor diameter. Higher void fraction in the smaller reactor diameter results in less biofilm surface area available and less cell density for the substrate to contact with the cells. Moreover, a higher void fraction can lead to channeling, where the substrate may flow preferentially through the voids without interacting with the cells [27,31]. The reactor length (Figure 7(c)) remains relatively consistent across all reactor diameters. Meanwhile, reactor volume (Figure 7(d)) varies significantly, showing a direct proportionality with reactor diameter.

The productivity value (Figure 7(e)) and the pressure drop (Figure 7(e)) are directly proportional to reactor diameter and inversely proportional to void fraction. As previously explained, a large void fraction in the smaller reactor diameter (volume) causes the surface area of the biofilm to also decrease [27]. A biofilm surface area that is too low causes the substrate contact area with the biofilm in the reactor to be lower, which leads to a decrease in productivity [31]. Furthermore, higher void fraction creating more open fluid flow paths, reducing frictional resistance and energy loss, resulting in the lower pressure drop.

3.2.6. Influence of solid particle diameter on reactor design and performance

The influence of solid particle diameter on reactor design and performance is shown in Figure 8 (Table S6, Supporting Information (SI)). The solid particle diameter value is directly proportional to the void fraction (Table S6) but is not significantly different. As previously explained, a solid particle diameter value that is too large can cause the void fraction value to increase [32]. However, the insignificant difference in void fraction indicates that the solid particle diameter in the range of 10-30 mm is relatively suitable for use in a reactor diameter of 20 cm.

Based on Figure 8(a), Figure 8(b), Figure 8(c), and Figure 8(d), the values of residence time, reactor length, and reactor volume are directly proportional to the solid particle diameter (and void fraction). As previously explained, increasing the solid particle diameter will cause an increase in the void fraction [32], decreasing the surface area of the biofilm. The lower surface area of the biofilm at a large solid particle diameter causes the contact location of the substrate with the biofilm in the reactor to be lower [31], which leads

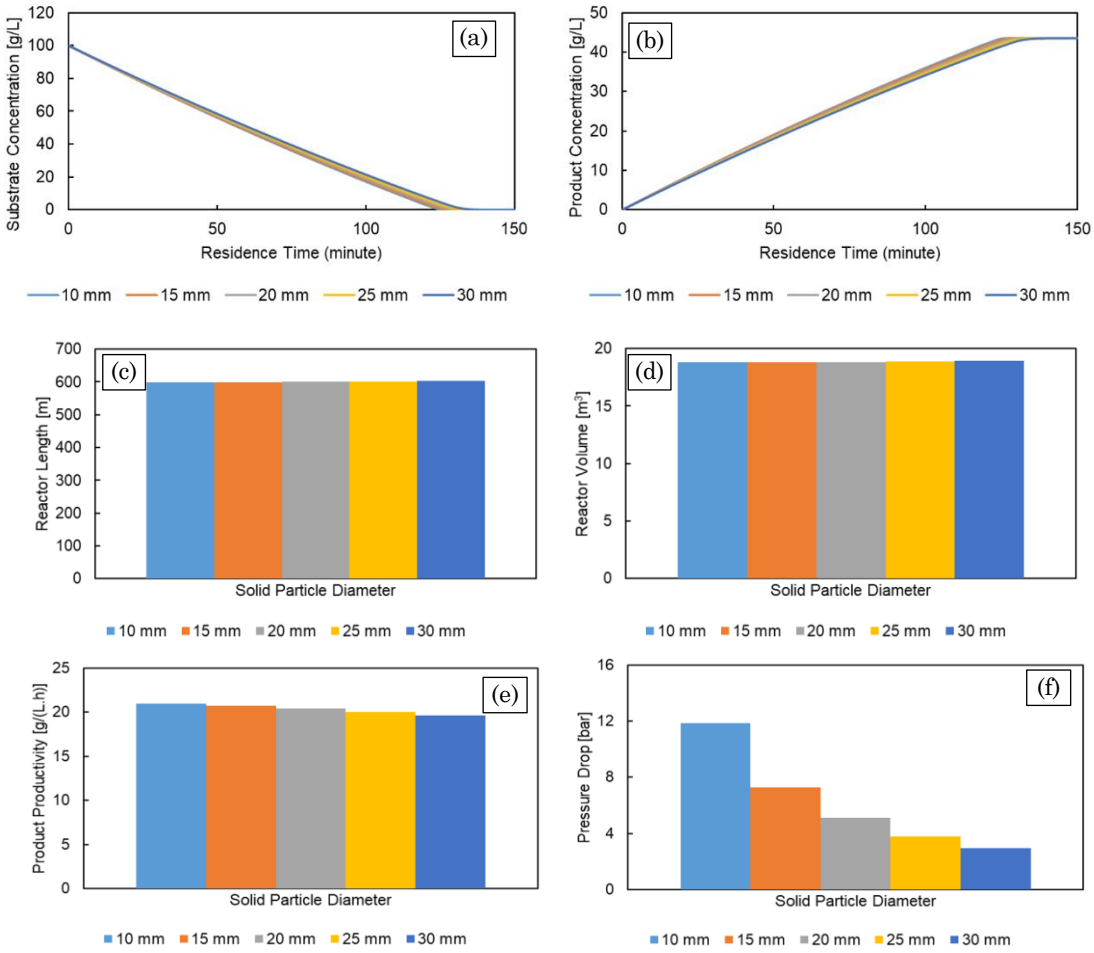

Figure 8. Influence of solid particle diameter on (a) substrate concentration profile, (b) product concentration profile, (c) reactor length at 99% conversion, (d) reactor volume at 99% conversion, (e) product productivity at 99% conversion, and (f) pressure drop at 99% conversion.

to an increase in the residence time, reactor length, and reactor volume.

According to productivity (Figure 8(e)) and pressure drop (Figure 8(f)), the productivity value and pressure drop are inversely proportional to the solid particle diameter (and void fraction). As previously explained, this occurs due to a decrease in the surface area of the biofilm at a high void fraction [32], leading to a decrease in productivity. Meanwhile, the larger void fraction creates more open fluid flow paths, reducing frictional resistance and energy loss in large solid particle diameter variation.

3.3 Sensitivity Analysis of Various Parameters on Reactor Design and Performance

Input parameter sensitivity analysis is carried out to identify input parameters that are sensitive to an output parameter. This is necessary to know the parameters that are important to manipulate to obtain good output parameters. Sensitivity analysis is shown in Figure 9. Figure 9(a) shows the sensitivity of input parameters to product concentration. Based on Figure 9(a), the parameter that is sensitive to product concentration is the initial substrate concentration. This happens because a high initial

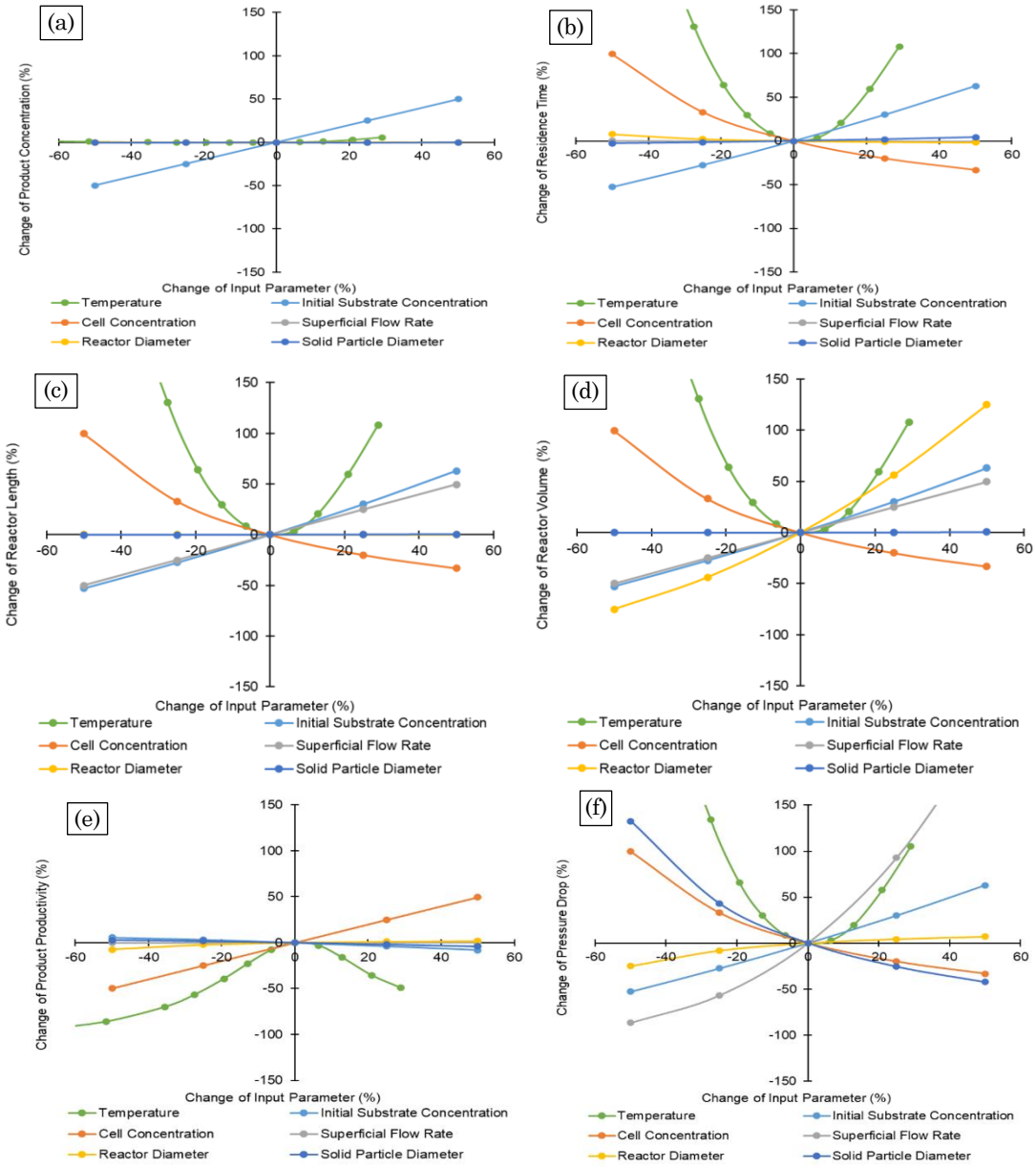

Figure 9. Sensitivity analysis of various input parameters on: (a) product concentration, (b) residence time, (c) reactor length, (d) reactor volume, (e) product productivity, and (f) pressure drop. The input parameter range is 22.5 – 40 °C for the temperature and -50% – 50% of the default condition for other input parameters, namely initial substrate concentration of 50 – 150 g/L, cell concentration of 3.75 – 11.25 g/L, superficial flow rate of 1.6 cm/s – 4.8 cm/s, reactor diameter of 10 cm – 30 cm, and solid particle diameter of 10 – 30 mm.

substrate concentration produces a high product concentration at the same conversion. This shows that to obtain a high product concentration, the initial substrate concentration needs to be increased, but this results in a higher residence time and reactor volume. Apart from that, Figure 9(a) also shows that temperature does not have a significant impact on changes in product concentration.

Figure 9(b) shows the sensitivity of input parameters to residence time. Based on Figure 9(b), parameters that are sensitive to residence time are temperature, initial substrate concentration, and cell concentration. This shows that temperature is very sensitive to residence time, meaning that fermentation must be carried out at the optimum temperature. Although product yield can increase at temperatures far from the optimum [30], temperature selection must still be made at the optimum growth temperature, and not at product yield. This corresponds with Khoja *et al.* which shows that fermentation temperature significantly influences the reaction time [33]. In addition, sensitivity analysis also shows that a high initial substrate concentration will require a high residence time. This corresponds with Pamphile *et al.* which shows that reactant concentration in plug flow reactor contributes significantly to reactor volume, which identical to reactor length and residence time [34]. Moreover, the result shows that a high amount of biocatalyst is needed to shorten the residence time. This corresponds with Vega *et al.* which shows that higher biomass concentration leads to a faster reaction rate [20].

Figure 9(c) shows the sensitivity of input parameters to reactor length. Based on Figure 9(c), the parameters that are sensitive to reactor length are temperature, initial substrate concentration, cell concentration, and superficial flow rate, with the parameters of temperature, initial substrate concentration, and cell concentration having identical tendencies to the residence time sensitivity analysis. This sensitivity analysis shows that the superficial flow rate needs to be kept low to reduce the reactor length. This corresponds with Maklavany *et al.* which shows that a higher superficial velocity of feed will result in a longer reactor length [35].

Figure 9(d) shows the sensitivity of input parameters to reactor volume. Based on Figure 9(d), parameters that are sensitive to reactor volume are temperature, initial substrate concentration, cell concentration, superficial flow rate, and reactor diameter, with the parameters of temperature, initial substrate concentration, cell concentration, and superficial flow rate having an identical trend with reactor length sensitivity analysis. This sensitivity analysis shows that a reactor diameter that is too large can increase the reactor volume significantly. However, the reactor diameter is not sensitive to residence time and reactor length, which means that the reactor diameter is not a parameter that will significantly influence the reaction rate, because in plug flow reactors, the residence time is much more influenced by the reactor length rather than reactor diameter [13].

Figure 9(e) shows the sensitivity of input parameters to product productivity. Based on Figure 9(e), parameters that are sensitive to productivity are temperature and cell concentration. This sensitivity analysis explains clearly that the temperature selection must be made at the optimum growth temperature. This corresponds with Khoja *et al.* which shows that optimum fermentation temperature significantly affects the reaction time, resulting in better productivity [33]. In addition, cell concentration must also be increased significantly to obtain high productivity. This corresponds with Vega *et al.* which shows that higher biomass concentration leads to a faster reaction rate, resulting in higher productivity [20].

Figure 9(f) shows the sensitivity of input parameters to pressure drop. According to Figure 9(f), all parameters are sensitive to pressure drop, with the reactor diameter being the least sensitive parameter. This sensitivity analysis indicates the importance of optimizing reactor operating conditions and configurations to manage the pressure drop. The pressure drop analysis and optimization of reactor configuration is shown in Supplementary Information (SI).

3.4 Further Considerations

This research provides potential manipulated parameters which are needed in the large-scale applications of anaerobically *S. cerevisiae* bioethanol fermentation, namely temperature, initial substrate concentration, cell concentration, superficial flow rate, reactor diameter, and solid particle diameter. Furthermore, the calculation method used in this study can be examined and implemented in other microbial systems in the bioprocess industry, such as lactic acid production, amino acid production, wastewater treatment, etc. However, there are several weaknesses of the continuous fixed bed biofilm plug flow reactor, such as pressure drop, temperature, and pH control. In a stirred tank reactor, the pressure drop is low, and the temperature and pH are easy to control by the cooling coil and heating jacket, because of the mixing process. In a plug flow reactor, the pressure drop and temperature increases while the pH decreases throughout the reactor. To solve this problem, a pump, cooling jacket, and base solution dosing must be made in an optimum placement on the reactor, so the pressure drop can be handled, and the temperature and pH

fluctuation are still in the tolerable range. Hence, it is recommended to study the design of the pumping system, cooling system, and pH control of the continuous fixed bed biofilm plug flow reactor.

In this research, the calculation process consists only of the reactor system. Whereas, to optimize the process, it is important to consider the supporting systems, the inoculum preparation, and the downstream processing. For example, to achieve thicker biofilm in the bed, the substrate used to produce the inoculum must be calculated and prepared. Moreover, to shorten the reactor length, the substrate concentration in the feed must be reduced, and this can lead to higher energy in ethanol purification and higher wastewater production. Whereas, bioethanol is a renewable energy, so it is important to maintain the energy used and wastewater produced lower to achieve the environmentally friendly concept. Hence, it is recommended to do a further study regarding the application of the reactor on the plant scale, which involves all the plant sectors, such as substrate preparation, inoculum preparation, fermentation, downstream processing, energy generation, and waste treatment.

4. Conclusion

This work studies reaction kinetics and mass transfer in continuous fixed bed biofilm plug flow reactor modelling to predict anaerobically bioethanol fermentation performance by *Saccharomyces cerevisiae* to provide an overview of the potential manipulated parameters on bioreactor operation, which lead to reaction rates, bioreactor design (dimensions), product productivity, and pressure drop. According to the study, the most sensitive parameters related to product productivity are temperature and cell concentration, so in its implementation, the temperature must be controlled at its optimum temperature and the inoculum must be prepared with high cell concentration. However, continuous fixed bed biofilm plug flow reactors have some limitations, such as high-pressure drop, which can be handled by decreasing the initial substrate concentration or adding pumps between the series reactors. Moreover, it is difficult to maintain the temperature and pH because the temperature and pH change throughout the reactor. Furthermore, this study only focused on the reactor system, whereas it is important to consider the supporting systems, such as inoculum preparation, downstream processing, and energy generation in the plant. Hence, for the next study, it is important to learn the optimization of the continuous fixed bed biofilm plug flow reactor design and operation, such as the pumping system, cooling system, and pH control of the reactor. Moreover, it is encouraged to study the implementation of the reactor on the plant scale.

Acknowledgment

The authors would gratefully acknowledge the scholarship funding from Indonesia Endowment Funds for Education (LPDP), Indonesian Ministry of Finance, Indonesia with the contract number of 202207210109892 (Christian Aslan).

CRedit Author Statement

Author Contributions: C. Aslan: Conceptualization, Methodology, Software, Investigation, Data Curation, Writing – Original Draft, Visualization; H. Devianto: Resources, Writing – Review & Editing; V. Wonoputri: Resources, Writing – Review & Editing; A. Harimawan: Resources, Supervision, Project Administration. All authors have read and agreed to the published version of the manuscript.

References

[1] Tse, T.J., Wiens, D.J., Reaney, M.J.T. (2021). Production of bioethanol—A review of factors affecting ethanol yield. *Fermentation*, 7(4), 268. DOI: 10.3390/fermentation7040268.

[2] Indonesian National Standardization Unit (2022). SNI 7390:2022 – Denaturated Bioethanol for Gasohol [Real Title: SNI 7390:2022 – Bioetanol Terdenaturasi untuk Gasohol]. Jakarta: Indonesian National Standardization Unit.

[3] Khuong, L.S., Masjuki, H.H., Zulkifli, N.W.M., Mohamad, E.N., Kalam, M.A., Alabdulkarem, A., Arslan, A., Mosarof, M.H., Syahir, A.Z., Jamshaid, M. (2017). Effect of gasoline–bioethanol blends on the properties and lubrication characteristics of commercial engine oil. *RSC Advances*, 7(25), 15005–15019. DOI: 10.1039/C7RA00357A.

[4] Wibowo, C.S., Sugiarto, B., Zikra, A., Budi, A., Mulya, T., Maymuchar (2018). The effect of gasoline-bioethanol blends to the value of fuel's octane number. *E3S Web of Conferences*, 67, 02033. DOI: 10.1051/e3sconf/20186702033.

[5] Sitorus, T.B., Siagian, J.A.R., Christopel, B. (2020). Study on the performance of the Otto engine by using mixtures of gasoline-bioethanol of nira. *IOP Conference Series: Materials Science and Engineering*, 725(1), 012015. DOI: 10.1088/1757-899X/725/1/012015.

[6] Cantarella, H., Leal Silva, J.F., Nogueira, L.A.H., Maciel Filho, R., Rossetto, R., Ekbom, T., Souza, G.M., Mueller-Langer, F. (2023). Biofuel technologies: Lessons learned and pathways to decarbonization. *GCB Bioenergy*, 15(10), 1190–1203. DOI: 10.1111/gcbb.13091.

[7] Ajanovic, A., Haas, R. (2014). On the future prospects and limits of biofuels in Brazil, the US and EU. *Applied Energy*, 135, 730–737. DOI: 10.1016/j.apenergy.2014.07.001.

[8] Roddy, D.J. (2012). Biomass and biofuels – Introduction. In: Sayigh, A. (ed) *Comprehensive Renewable Energy*. Elsevier, pp. 1–9. DOI: 10.1016/B978-0-08-087872-0.00501-1.

[9] Altieri, A. (2012). Bioethanol Development in Brazil. In: Sayigh, A. (ed) *Comprehensive Renewable Energy*. Elsevier, pp. 15–26. DOI: 10.1016/B978-0-08-087872-0.00504-7.

[10] Hartmann, F.S.F., Udugama, I.A., Seibold, G.M., Sugiyama, H., Gernaey, K. V. (2022). Digital models in biotechnology: Towards multi-scale integration and implementation. *Biotechnology Advances*, 60, 108015. DOI: 10.1016/j.biotechadv.2022.108015.

[11] Villadsen, J., Nielsen, J., Lidén, G. (2011). *Bioreaction Engineering Principles*. New York: Springer.

[12] Aslan, C., Devianto, H., Wonoputri, V., Harimawan, A. (2023). Study of cell elemental balance and cell thermodynamics in microorganism black box modeling: Prediction of bioethanol fermentation stoichiometry by *Saccharomyces cerevisiae* as a function of temperature. In: *International Seminar on Chemical, Food, and Chemurgy Engineering Soehadi Reksowardojo*. Bandung:

[13] Fogler, H.S. (2016). *Elements of Chemical Reaction Engineering*. USA: Prentice Hall.

[14] Praj (2024). Advanced Bioethanol. In: https://www.praj.net/businesslines/advanced-bioethanol/.

[15] Tomsa Destil (2024). Ethanol. In: https://tomsadestil.es/en/etanol/.

[16] Vogelbusch (2024). Bioethanol Technology. In: https://www.vogelbusch-biocommodities.com/en/technology/alcohol-process-plants/bioethanol-technology/.

[17] Espinosa-Ortiz, E.J., Gerlach, R., Peyton, B.M., Roberson, L., Yeh, D.H. (2023). Biofilm reactors for the treatment of used water in space:potential, challenges, and future perspectives. *Biofilm*, 6, 100140. DOI: 10.1016/j.bioflm.2023.100140.

[18] Lindeque, R., Woodley, J. (2019). Reactor selection for effective continuous biocatalytic production of pharmaceuticals. *Catalysts*, 9(3), 262. DOI: 10.3390/catal9030262.

[19] Animia A, W., Chidinma T, E. (2020). Performance evaluation of PFR and CSTR 1-reactor tank for formaldehyde petrochemical production. *International Journal of Chemical and Process Engineering Research*, 7(1), 18–45. DOI: 10.18488/journal.65.2020.71.18.45.

[20] Vega, J.L., Clausen, E.C., Gaddy, J.L. (1988). Biofilm reactors for ethanol production. *Enzyme and Microbial Technology*, 10(7), 390–402. DOI: 10.1016/0141-0229(88)90033-6.

[21] Sharma, V., Mishra, H.N. (2014). Unstructured kinetic modeling of growth and lactic acid production by *Lactobacillus plantarum* NCDC 414 during fermentation of vegetable juices. *LWT - Food Science and Technology*, 59(2), 1123–1128. DOI: 10.1016/j.lwt.2014.05.039.

[22] Cui, Y., Liu, R., Xu, L., Zheng, W., Sun, W. (2018). Fermentation kinetics of enzymatic hydrolysis bagasse solutions for producing L-lactic acid. *Sugar Tech*, 20(3), 364–370. DOI: 10.1007/s12355-018-0592-4.

[23] Damayanti, A., Bahlawan, Z.A.S., Kumoro, A.C. (2022). Modeling of bioethanol production through glucose fermentation using *Saccharomyces cerevisiae* immobilized on sodium alginate beads. *Cogent Engineering*, 9(1) DOI: 10.1080/23311916.2022.2049438.

[24] Shuler, M.L., Kargi, F., DeLisa, M.P. (2017). *Bioprocess Engineering: Basic Concepts*, 3rd ed. Upper Saddle River: Prentice Hall.

[25] Bird, R.B., Stewart, W.E., Lightfoot, E.N. (2002). *Transport Phenomena*. New York: John Wiley & Sons.

[26] Germec, M., Turhan, I., Karhan, M., Demirci, A. (2019). Kinetic modeling and techno-economic feasibility of ethanol production from carob extract based medium in biofilm reactor. *Applied Sciences*, 9(10), 2121. DOI: 10.3390/app9102121.

[27] Benyahia, F., O'Neill, K.E. (2005). Enhanced voidage correlations for packed beds of various particle shapes and sizes. *Particulate Science and Technology*, 23(2), 169–177. DOI: 10.1080/02726350590922242.

[28] Geankoplis, C.J. (1993). *Transport Processes and Unit Operations*. New Jersey: Prentice Hall.

[29] Stewart, P.S. (2003). Diffusion in biofilms. *Journal of Bacteriology*, 185(5), 1485–1491. DOI: 10.1128/JB.185.5.1485-1491.2003.

[30] Zakhartsev, M., Yang, X., Reuss, M., Pörtner, H.O. (2015). Metabolic efficiency in yeast *Saccharomyces cerevisiae* in relation to temperature dependent growth and biomass yield. *Journal of Thermal Biology*, 52, 117–129. DOI: 10.1016/j.jtherbio.2015.05.008.

[31] Wu, C., Tanaka, K., Tani, Y., Bi, X., Liu, J., Yu, Q. (2022). Effect of particle size on the colonization of biofilms and the potential of biofilm-covered microplastics as metal carriers. *Science of The Total Environment*, 821, 153265. DOI: 10.1016/j.scitotenv.2022.153265.

[32] Negri, M., Wilhelm, M., Hendrich, C., Wingborg, N., Gediminas, L., Adelöw, L., Maleix, C., Chabernaud, P., Brahmi, R., Beauchet, R., Batonneau, Y., Kappenstein, C., Koopmans, R.-J., Schuh, S., Bartok, T., Scharlemann, C., Gotzig, U., Schwentenwein, M. (2018). New technologies for ammonium dinitramide based monopropellant thrusters – The project RHEFORM. *Acta Astronautica*, 143, 105–117. DOI: 10.1016/j.actaastro.2017.11.016.

[33] Khoja, A.H., Ali, E., Zafar, K., Ansari, A.A., Nawar, A., Qayyum, M. (2015). Comparative study of bioethanol production from sugarcane molasses by using *Zymomonas mobilis* and *Saccharomyces cerevisiae*. *African Journal of Biotechnology*, 14, 2455–2462. DOI: 10.5897/AJB2015.14569

[34] Pamphile, B.N., Ndjibu, N.J., Vanshok, E., Gédéon, E.N. (2022). Modeling and simulation of reactors in plug flow reactor (PFR) and Packed Bed Reactor (PBR) series for the conversion of methanol into hydrocarbons. *African Journal of Environmental Science and Technology*, 16(8), 286–294. DOI: 10.5897/AJEST2022.3091.

[35] Maklavany, D.M., Shariati, A., Khosravi-Nikou, M.R., Roozbehani, B. (2017). Hydrogen production via low temperature water gas shift reaction: Kinetic study, mathematical modeling, simulation and optimization of catalytic fixed bed reactor using gPROMS. *Chemical Product and Process Modeling*, 12(3). DOI: 10.1515/cppm-2016-0063.

[36] Zempléni, A., Hansen, B.W., KiØrboe, T., Ryderheim, F. (2022). Resolving the paradox of the ambush feeding cyclopoid copepod *Apocyclops royi* being microphageous. *Journal of Plankton Research*, 44(6), 936–941. DOI: 10.1093/plankt/fbac040.